Deep Gaussian Process Proximal Policy Optimization

Matthijs van der Lende
University of Groningen
m.r.van.der.lende@student.rug.nl

Juan Cardenas-Cartagena
University of Groningen
j.d.cardenas.cartagena@rug.nl

Abstract

Uncertainty estimation for Reinforcement Learning (RL) is a critical component in control tasks where agents must balance safe exploration and efficient learning. While deep neural networks have enabled breakthroughs in RL, they often lack calibrated uncertainty estimates. We introduce Deep Gaussian Process Proximal Policy Optimization (GPPO), a scalable, model-free actor-critic algorithm that leverages Deep Gaussian Processes (DGPs) to approximate both the policy and value function. GPPO maintains competitive performance with respect to Proximal Policy Optimization on standard high-dimensional continuous control benchmarks while providing well-calibrated uncertainty estimates that can inform safer and more effective exploration.

1 Introduction

Reinforcement Learning (RL) concerns itself with solving sequential decision problems by learning how to act in an environment such that a given reward signal is maximized. A central challenge in modern RL, particularly in continuous state-action domains, lies in balancing effective exploration with efficient learning from in safety-critical environments with limited data. While deep neural networks have enabled relevant advances in RL [Mnih et al., 2015, Wang et al., 2016, Schulman et al., 2017], they lack uncertainty estimate out-of-the-box, which is key for safe and efficient exploration [Lockwood and Si, 2022].

Uncertainty estimation plays a pivotal role in RL by enabling agents to quantify their confidence in predictions, thereby guiding exploration strategies. For instance, in regions of high uncertainty, an agent can prioritize exploration to gather more data or decide not to take action if the uncertainty is too high and taking action could be unsafe, while in well-understood regions, it can exploit learned knowledge. Gaussian Processes (GPs) output well-calibrated predictive distributions [Anonymous, 2025b, Murphy, 2023], capturing both epistemic and aleatoric uncertainty in a Bayesian framework. This allows RL agents to make informed decisions based on the confidence of their value function or policy estimate. Deep Gaussian Processes (DGPs) extend this capability by hierarchically composing GPs [Damianou and Lawrence, 2013], enabling more flexible and expressive representations while retaining uncertainty estimation. These properties make GPs and DGPs particularly suitable for RL applications requiring safe and interpretable decision-making, such as robotics and healthcare.

1.1 Related Work

Previous work combing GPs and RL primarly focused on estimating the world model (e.g., transition and reward function) [Rasmussen and Kuss, 2003, Kamthe and Deisenroth, 2018] or value functions [Engel et al., 2005, Chowdhary et al., 2014, Kameda and Tanaka, 2023]. In particular Engel et al. [2005] used GPs to approximated both the value and action-value function, resulting in a variant of the SARSA algorithm. This approach was extended to the off-policy case by Chowdhary et al. [2014].

Preprint.

Rao et al. [2020] used a GP as the critic for Proximal Policy Optimization (PPO), learning the expected return of a policy given its parameters and used the expected improvement acquisition function to encourage exploration instead of an entropy term, resulting in empirically comparable or better performance than vanilla PPO. Berkenkamp [2019] showed other uses of GPs for safe RL, where the policy must stay within a "safe" region of the state space. One model-free approach used GPs to model the policy objective and leveraged the GP predictive mean and confidence intervals to enforce safety constraints on the policy parameters.

These methods were limited to low dimensional/complexity environments due to the computational complexity of standard GP regression ($O(N^3)$ time and $O(N^2)$ space for an N-size dataset) [Rasmussen and Williams, 2019]). Recent advances in scalable GP methods, such as inducing point methods [Titsias, 2009] and deep GP architectures [Damianou and Lawrence, 2013, Jankowiak et al., 2020], have significantly improved the scalability and applicability of GPs for data-intensive applications. For example, Salimbeni and Deisenroth [2017] introduced doubly stochastic variational inference for DGPs, enabling efficient training on large datasets. Additionally, Jankowiak et al. [2020] proposed Deep Sigma Point Processes (DSPPs), DGPs that make use of learnable quadrature rules to propagate uncertainty as opposed to Monte Carlo sampling, which empirically offers better-calibrated uncertainty estimates. These advancements make GPs a more viable option for modern RL tasks. In particular, Anonymous [2025a] used these recent scalable methods for DGP regression for estimating the action-value function, but this framework has not been extended to DSPPs or to estimating the policy directly.

1.2 Contributions

This work introduces a scalable model-free actor-critic algorithm, Deep Gaussian Process Proximal Policy Optimization (GPPO), based on PPO that uses DGPs to directly approximate both the policy and the value function. GPPO achieves competitive performance to PPO while providing calibrated uncertainty estimates for exploration.

2 Background

2.1 Gaussian Processes

A GP is a collection of real-valued random variables $\{f(\mathbf{x}) : \mathbf{x} \in \mathcal{X}\}$ such that any finite subset has a joint Gaussian distribution [Rasmussen and Williams, 2019, Murphy, 2023]. A GP $f(\mathbf{x}) \sim \mathcal{GP}(m(\mathbf{x}), k(\mathbf{x}, \mathbf{x}'))$ is fully characterized by a mean $m(\mathbf{x}) = \mathbb{E}[f(\mathbf{x})]$ and covariance function $k(\mathbf{x}, \mathbf{x}') = \mathbb{E}[(f(\mathbf{x}) - m(\mathbf{x}))(f(\mathbf{x}') - m(\mathbf{x}'))]$, e.g., the radial basis function kernel. The kernel encodes prior assumptions about function behavior by defining similarity between inputs. A GP provides Bayesian nonparametric regression with inherent uncertainty quantification by considering $\mathcal{X}$ as the domain of a function $h : \mathcal{X} \to \mathbb{R}$ that we want to approximate. Conditioning on data $\mathcal{D} = \{(\mathbf{x}_i, y_i)\}_{i=1}^N$ yields an analytic predictive posterior distribution $p(y|\mathbf{x}, \mathcal{D})$, but exact inference requires an $O(N^3)$ covariance matrix inversion.

The key takeaway about DGPs and inducing point methods is that we can stack GPs hierarchically, and methods based on variational inference exist that make this tractable [Salimbeni and Deisenroth, 2017, Jankowiak et al., 2020]. This introduces a set of variational parameters ϕ, which we can optimize using stochastic gradient descent. The parameters ϕ include likelihood parameters such as Gaussian observation noise, and for each GP, kernel hyperparameters, a set of inducing points with associated inducing variable outputs that provide a sparse, low-rank approximation of the full dataset to condition on, and a variational distribution over inducing variables $q(\mathbf{u}) \approx p(\mathbf{u}|\mathcal{D})$ used to compute an approximate posterior predictive distribution. For N training samples, M inducing points, and D^i GPs in layer i, DGPs have time complexity $O(NM^2 \sum D^i)$ and space complexity $O((NM + M^2) \sum D^i)$ [Murphy, 2023].

2.2 Reinforcement Learning

The environment is modeled as a Markov Decision Process (MDP) $\mathcal{M} = (\mathcal{S}, \mathcal{A}, p, r, \gamma)$ where $\mathcal{S} \subseteq \mathbb{R}^n$ is the state space and $\mathcal{A} \subseteq \mathbb{R}^m$ is the action space. $\gamma \in (0, 1]$ is the discount factor. $p(s'|s, a)$ is the transition distribution of the environment and $r : \mathcal{S} \times \mathcal{A} \to \mathbb{R}$ is a reward function. The agent interacts with the environment through its policy $\pi(a|s)$, which is a conditional probability

distribution of the actions given the state. For continuous action spaces a common representation is a multivariate Gaussian distribution:

$$\pi(a|s;\theta) = \mathcal{N}(a|\mu_\theta(s), \Sigma_\theta(s)), \tag{1}$$

where $\mu_\theta(s) \in \mathbb{R}^m, \Sigma_\theta(s) = \text{diag}(\sigma^2_\theta(s))$ are the mean and variance outputs of a parametric function approximator with parameters $\theta \in \mathbb{R}^p$.

3 Gaussian Process Proximal Policy Optimization

We introduce GPPO by extending the standard objective for DSPPs to the actor–critic framework of PPO. DSPPs are variants of DGPs [Jankowiak et al., 2020] that replace Monte Carlo sampling with learned quadrature rules to deterministically propagate uncertainty through the layers. Instead of sampling latent variables, DSPPs use a fixed number of sigma points, whose positions and weights are learnable. This yields a finite mixture approximation to the predictive distribution:

$$p_{\text{dspp}}(\mathbf{y}|\mathbf{x}) = \sum\nolimits_{j=1}^{Q} \omega^{(j)} p^{(j)}(\mathbf{y}|\mathbf{x}) \tag{2}$$

where Q is the number of quadrature sites with weights $\omega^{(j)}$. The training objective for set of data samples $\{(\mathbf{x}_i, \mathbf{y}_i)\}_{i=1}^N$ becomes:

$$\mathcal{L}_{\text{dspp}}(\phi) = \sum_{i=1}^{N} \log p_{\text{dspp}}(\mathbf{y}_i|\mathbf{x}_i) - \beta\mathcal{L}_{\text{KL}} \tag{3}$$

where:

$$\mathcal{L}_{\text{KL}} = \sum_{l=1}^{L} D_{\mathbb{KL}}[q(\mathbf{U}^l)\|p(\mathbf{U}^l|\mathbf{Z}^{l-1})]. \tag{4}$$

where $q(\mathbf{U}^l)$ and $p(\mathbf{U}^l|\mathbf{Z}^{l-1})$ are the variational and prior distributions over the inducing variables at layer l, respectively. $\beta > 0$ is a regularization constant.

A GP computes a predictive posterior distribution conditioned on the input. The policy is a conditional distribution on the state, so if we use our DGP to model the policy then the notation changes as follows:

$$\mathcal{L}(\phi) = \hat{\mathbb{E}}_t[\log \pi(a_t|s_t;\phi)] - \beta\mathcal{L}_{\text{KL}}, \tag{5}$$

where we replace the sum by $\hat{\mathbb{E}}_t[z_t] := \frac{1}{T}\sum_{t=1}^{T} z_t$.

We now rewrite (5) to include the PPO specific changes, such as the clipping of the surrogate objective:

$$\mathcal{L}(\phi) = \hat{\mathbb{E}}_t[\min(r_t(\phi)\hat{A}_t, \text{clip}(r_t(\phi), 1-\epsilon, 1+\epsilon)\hat{A}_t) - c_1\mathcal{L}^{\text{VF}}_t(\phi) + c_2 S[\pi_\phi](s_t)] - \beta\mathcal{L}_{\text{KL}}. \tag{6}$$

where $\mathcal{L}^{\text{VF}}$ is a surrogate loss for learning the value function and $S[\pi_\phi]$ a entropy regularization term for promoting exploration. $r_t(\phi)$ is the the ratio of the predictive posterior distributions over actions:

$$r_t(\phi) = \frac{\pi(a_t|s_t;\phi)}{\pi_{\text{old}}(a_t|s_t;\phi)} = \log \pi(a_t|s_t;\phi) - \log \pi_{\text{old}}(a_t|s_t;\phi). \tag{7}$$

The Generalized Advantage Estimator (GAE) [Schulman et al., 2018] $\hat{A}_t$ is calculated as usual. Given a value function estimate $V : \mathcal{S} \to \mathbb{R}$, compute the TD error $\delta_t = r_t + \gamma V(s_{t+1}) - V(s_t)$. Then the GAE is:

$$\hat{A}_t = \sum_{\ell=0}^{\infty} (\gamma\lambda)^\ell \delta_{t+\ell} = \delta_t + \gamma\lambda\hat{A}_{t+1}. \tag{8}$$

Here $\lambda \in [0, 1]$ is a regularization hyperparameter with larger values decreasing bias but increasing variance. The temporal difference target V_t^{target} can be computed from the GAE as $V_t^{\text{target}} = \hat{A}_t + V(s_t)$.

Because GPPO leverages the same $\mathcal{L}^{\text{CLIP}}$ objective as PPO it inherits the same theoretical properties under the mirror learning framework [Grudzien et al., 2022]. Which includes (in expectation) strict monotonic policy improvement and the convergence of the value function to the optimal one. We summarize the complete GPPO training loop in Algorithm 1 for clarity.

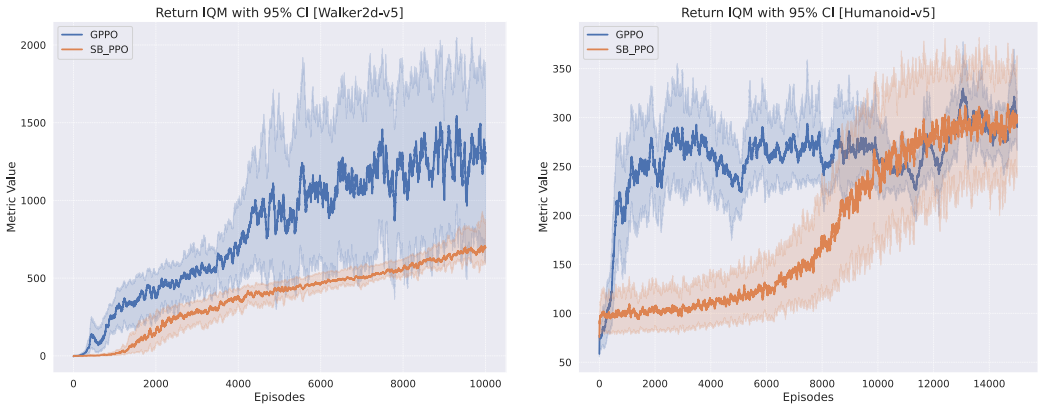

Figure 1: Reward curves (with a 50-step smoothing window) comparing the PPO implementation from Stablebaselines3 and GPPO in Walker2D (left) and Humanoid (right). Results show IQM returns with 95% CIs across 3 runs.

3.1 Estimating the Value Function

Estimating the value function $V^\pi : \mathcal{S} \to \mathbb{R}$ requires some care, just like with neural networks, we can use two outputs heads for estimating π and V^π, but this time using GPs instead of perceptrons. However if we use the squared error loss we do not get well calibrated probability distributions as it is not a proper scoring rule which actively incentivizes modeling the true distribution. To remedy this we will formulate the value function objective as maximizing a log likelihood:

$$\mathcal{L}^{\text{VF}}(\phi) = \hat{\mathbb{E}}_t[\log p_{\text{dspp}}(V_t^{\text{target}} | s_t; \phi)]. \tag{9}$$

Here implicitly we assume the value function GP head is used in this expression. To show that (9) is a valid loss function for learning the vale function we can write out the likelihood

$$p(V_t^{\text{target}} | s_t) = \mathcal{N}(V_t^{\text{target}} | \mu(s_t), \sigma^2(s_t)). \tag{10}$$

For simplicity we assume its a single Gaussian, but for DSPPs this becomes a Gaussian mixture. The log-likelihood for a Gaussian is:

$$\log p(V_t^{\text{target}} | s_t) = -\frac{1}{2}\log(2\pi\sigma^2(s_t)) - \frac{(V_t^{\text{target}} - \mu(s_t))^2}{2\sigma^2(s_t)}. \tag{11}$$

Maximizing the log-likelihood is equivalent to minimizing the negative log likelihood which corresponds to minimizing:

$$\underbrace{\frac{(V_t^{\text{target}} - \mu(s_t))^2}{2\sigma^2(s_t)}}_{\text{weighted squared error}} + \underbrace{\frac{1}{2}\log\sigma^2(s_t)}_{\text{uncertainty regularization}}. \tag{12}$$

If the variance $\sigma^2(s_t)$ is fixed or treated as a constant, this reduces to minimizing the squared error between the target value and the predicted mean $(V_t^{\text{target}} - \mu(s_t))^2$. Hence, minimizing $-\mathcal{L}_t^{\text{VF}}$ with a Gaussian likelihood implicitly encourages the predicted mean state value $\mu(s_t)$ to fit V_t^{target} closely, i.e., it minimizes the squared error weighted by the predictive uncertainty.

Instead of computing advantages using only the mean prediction $\bar{V}_\phi(s)$, we propagate the state value uncertainty into the GAE and in turn the policy update by sampling from the value function posterior $\tilde{V}(s) \sim p_{\text{dspp}}(V^{\text{target}} | s, \phi)$. In uncertain states (where the value posterior has high variance), $\tilde{V}(s)$ varies widely. In well-known states (low variance), $\tilde{V}(s)$ stabilizes near the mean, favoring exploitation.

4 Results

We trained GPPO and PPO on continuous control tasks, Walker2D and Humanoid, from the Gymnasium library Towers et al. [2024]. Full experimental details, including hyperparameter tuning via

Algorithm 1 Deep Gaussian Process Policy Optimization

Require: `n_steps`: number of timesteps to interact with environment before updating, `n_envs`: number of environments to run in parallel, K: number of epochs, B: batch size, $\alpha > 0$: learning rate, $\gamma > 0$: discount factor, λ: GAE regularization, ϵ: clip range for $\mathcal{L}^{\text{CLIP}}$, $c_1 > 0, c_2 > 0$: value function and entropy term coefficients, $\|g\|_{\max}$: max gradient norm, M: number of inducing points, Q: number of quadrature sites, β: KL divergence scaling factor

Ensure: Trained DGP for jointly estimating $\pi(a|s;\phi) \approx \pi^*(a|s), \tilde{V}(s) \approx V^*(s)$

Initialize rolloutbuffer $\mathcal{D}$ with capacity `n_steps` $\cdot$ `n_envs`
for each layer in the DGP **do**
  for each GP **do**
    Initialize $f(\mathbf{x}) \sim \mathcal{GP}(m(\mathbf{x}), k(\mathbf{x}, \mathbf{x}'))$ with a constant mean function $m(\mathbf{x}) = C$ for the final layer and a linear mean function $m(\mathbf{x}) = \mathbf{w}^\top \mathbf{x} + b$ for all other layers, following Salimbeni and Deisenroth [2017]. Use an RBF covariance function $k(\mathbf{x}, \mathbf{x}') = \sigma_f^2 \exp(-\frac{|\mathbf{x}-\mathbf{x}'|^2}{2\ell^2})$ with length scale ℓ, output scale σ_f^2, and a Gaussian likelihood with observation noise σ_n^2. Initialize the inducing points by sampling from a standard normal distribution $\mathcal{N}(\mathbf{0}, \mathbf{I})$
  end for
end for
Initialize Adam [Kingma and Ba, 2017] with learnable (hyper)parameters ϕ and learning rate α.
Instantiate `n_env` parallel environments (e.g., in seperate processes/threads).
for iteration $1, 2, ...$ (stop when maximum number of episodes is reached) **do**
  for $t = 1, 2, ...,$ `n_steps` **do**
    $a_t \sim \pi(\cdot|s_t;\phi_{\text{old}}) = p(a_t|s_t;\phi_{\text{old}})$ [using batch computation w.r.t. `num_envs`]
    $\tilde{V}(s_t) \sim p(V^{\text{target}}|s_t;\phi)$ [see also Appendix C]
    $r_{t+1}, s_{t+1} \sim p(r_{t+1}, s_{t+1}|s_t, a_t)$, $d_{t+1} = \mathbb{I}[s_{t+1}$ is a terminal state]
    Add $(s_t, a_t, r_{t+1}, s_{t+1}, d_{t+1}, \log \pi(a_t|s_t;\phi_{\text{old}}), \tilde{V}(s_t))$ to rolloutbuffer $\mathcal{D}$
  end for
  Compute advantage estimates $\hat{A}_1^1, \ldots, \hat{A}_{\texttt{n\_steps}}^1, \ldots, \hat{A}_1^{\texttt{n\_envs}}, \ldots, \hat{A}_{\texttt{n\_steps}}^{\texttt{n\_envs}}$
  Sample uniformly with replacement from $\mathcal{D}$ and for each $B \leq$ `num_envs` $\cdot$ `n_steps` size minibatch optimize surrogate loss $\mathcal{L}(\phi)$ with Adam for K epochs.
  $\phi_{\text{old}} \leftarrow \phi$
end for

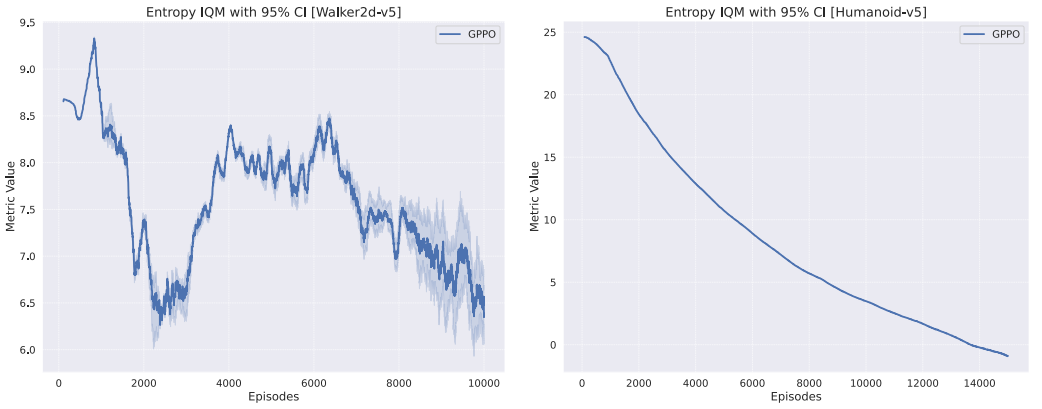

Figure 2: Entropy over training (with a 50-step smoothing window) for GPPO in Walker2D (left) and Humanoid (right). Curves show IQM with 95% confidence intervals across 3 runs. This curve highlights how the epistemic uncertainty captured by the entropy of the policy distribution decreases over time.

Bayesian optimization, are provided in Appendices A.1, A.2, and A.3. During hyperparameter tuning, multiple DGP architectures with varying depth, number of GPs per layer were trained.

The hyperparameters found by Bayesian optimization are given in Table 3. Figures 1 and 2 shows the reward and policy entropy curve on select Mujoco environments, showing the interquartile mean

Environment	Algorithm	Avg. Return $\pm$ Std. Dev.
Walker2d-v5	PPO	654.76 ± 117.30
	GPPO	1611.37 ± 686.14
Walker2d-v5 (modified gravity)	PPO	914 ± 357.08
	GPPO	480.27 ± 218.18
Humanoid-v5	PPO	300.41 ± 78.08
	GPPO	287.41 ± 20.9
Humanoid-v5 (modified gravity)	PPO	499.44 ± 199.25
	GPPO	625.62 ± 60.11

Table 1: Evaluation metrics for multiple environments comparing PPO and GPPO. Values are reported as mean $\pm$ standard deviation over 100 evaluation episodes. Modified gravity implies that default gravity vector $\mathbf{g} = (0, 0, -9.81)$ reflecting earths gravity is set to that of the moon $\mathbf{g}' = (0.0, 0.0, -1.62)$.

with a 95% bootstrapped confidence interval as described in Appendix A.3. We empirically show in Appendix B that while GPPO does scale to reasonably large environments (e.g., Humanoid), it is a constant factor more computationally expensive. Table 1 gives an estimate of how PPO/GPPO behave when the environment dynamics change after training.

In Walker2D, GPPO compares favorably to PPO, showing higher average performance at the end of training with a 2525.06 IQM mean return and a $(2155.19, 2904.04)$ confidence interval, compared to PPO's 742.16 IQM mean return with a $(686.73, 1081.71)$ interval. Compared to PPO, GPPO exhibits greater variance across runs.

In Humanoid, we observe a similar pattern with slightly different learning speeds. GPPO achieves an IQM return of 248.43 with a $(244.05, 252.62)$ confidence interval at the final episode. PPO achieves an IQM return of 349.64 with a $(321.42, 377.51)$ confidence interval. For Humanoid, the posterior distribution converges to a delta distribution as indicated by the entropy approaching zero. This is expected given that the entropy coefficient c_2 was set relatively low (8.7×10^{-5}) for GPPO compared to PPO ($c_2 = 2.38 \times 10^{-3}$). This behavior is related to the exploration-exploitation dilemma and can be controlled for via the c_2 parameter.

5 Discussion & Conclusion

GPPO demonstrates that DGPs can effectively replace neural networks in actor-critic frameworks while maintaining competitive performance. On standard continuous control benchmarks, GPPO achieves reward levels comparable to or better than PPO, with the added benefit of built-in uncertainty quantification via DGPs. These results show that modern GP approximations can be scaled to RL problems without sacrificing performance, at the cost of additional computation time.

Overall, both environments appear to benefit from using DGPs to model the policy and value function, particularly due to the inherent uncertainty quantification. As the agent learns and reward increases, the overall uncertainty captured by the entropy of the policy decreases accordingly. For Walker2D, GPPO's entropy at the final episode has an IQM of 6.27 with a $(5.82, 6.72)$ confidence interval.

Note that the performance differences between GPPO and PPO are subject to hyperparameter choice and the number of timesteps or episodes for which the agent is trained. These results are primarily intended to demonstrate that GPPO can scale to larger environments and compete with standard PPO.

Future work includes a theoretical analysis of modeling the policy and value functions as calibrated posterior distributions, and identifying further use cases for the predictive variance of the value function estimation. Experiments can also be extended to Partially Observable Markov Decision Processes (POMDPs) to evaluate the benefits of uncertainty quantification. Additional benchmarking in higher-dimensional environments is also needed to better understand the limitations of the algorithm.

References

Rishabh Agarwal, Max Schwarzer, Pablo Samuel Castro, Aaron C Courville, and Marc Bellemare. Deep Reinforcement Learning at the Edge of the Statistical Precipice. In *Advances in Neural Information Processing Systems*, volume 34, pages 29304–29320. Curran Associates, Inc., 2021. URL https://proceedings.neurips.cc/paper_files/paper/2021/hash/f514cec81cb148559cf475e7426eed5e-Abstract.html.

Anonymous. Interpretable function approximation with gaussian processes in value-based model-free reinforcement learning. In *Proceedings of the 6th Northern Lights Deep Learning Conference (NLDL)*, pages 141–154, 2025a. Author details omitted for double-blind review.

Anonymous. Evaluating uncertainty in deep gaussian processes, April 2025b. URL https://arxiv.org/abs/2504.17719. Author details omitted for double-blind review.

Felix Berkenkamp. Safe Exploration in Reinforcement Learning: Theory and Applications in Robotics. page 206 p. [object Object], 2019. doi: 10.3929/ETHZ-B-000370833. URL http://hdl.handle.net/20.500.11850/370833. Artwork Size: 206 p. Medium: application/pdf.

Girish Chowdhary, Miao Liu, Robert Grande, Thomas Walsh, Jonathan How, and Lawrence Carin. Off-policy reinforcement learning with Gaussian processes. *IEEE/CAA Journal of Automatica Sinica*, 1(3):227–238, July 2014. ISSN 2329-9274. doi: 10.1109/JAS.2014.7004680. URL https://ieeexplore.ieee.org/abstract/document/7004680. Conference Name: IEEE/CAA Journal of Automatica Sinica.

Andreas C. Damianou and Neil D. Lawrence. Deep Gaussian Processes, March 2013. URL http://arxiv.org/abs/1211.0358. arXiv:1211.0358 [cs, math, stat].

Yaakov Engel, Shie Mannor, and Ron Meir. Reinforcement learning with Gaussian processes. In *Proceedings of the 22nd international conference on Machine learning*, ICML '05, pages 201–208, New York, NY, USA, August 2005. Association for Computing Machinery. ISBN 978-1-59593-180-1. doi: 10.1145/1102351.1102377. URL https://doi.org/10.1145/1102351.1102377.

Jakub Grudzien, Christian A. Schroeder De Witt, and Jakob Foerster. Mirror Learning: A Unifying Framework of Policy Optimisation. In *Proceedings of the 39th International Conference on Machine Learning*, pages 7825–7844. PMLR, June 2022. URL https://proceedings.mlr.press/v162/grudzien22a.html. ISSN: 2640-3498.

Martin Jankowiak, Geoff Pleiss, and Jacob R. Gardner. Deep Sigma Point Processes, December 2020. URL http://arxiv.org/abs/2002.09112. arXiv:2002.09112 [stat].

Kiseki Kameda and Fuyuhiko Tanaka. Reinforcement learning with Gaussian process regression using variational free energy. *Journal of Intelligent Systems*, 32(1), January 2023. ISSN 2191-026X. doi: 10.1515/jisys-2022-0205. URL https://www.degruyter.com/document/doi/10.1515/jisys-2022-0205/html. Publisher: De Gruyter.

Sanket Kamthe and Marc Deisenroth. Data-Efficient Reinforcement Learning with Probabilistic Model Predictive Control. In *Proceedings of the Twenty-First International Conference on Artificial Intelligence and Statistics*, pages 1701–1710. PMLR, March 2018. URL https://proceedings.mlr.press/v84/kamthe18a.html. ISSN: 2640-3498.

Diederik P. Kingma and Jimmy Ba. Adam: A Method for Stochastic Optimization, January 2017. URL http://arxiv.org/abs/1412.6980. arXiv:1412.6980 [cs].

Owen Lockwood and Mei Si. A Review of Uncertainty for Deep Reinforcement Learning. *Proceedings of the AAAI Conference on Artificial Intelligence and Interactive Digital Entertainment*, 18(1):155–162, October 2022. ISSN 2334-0924. doi: 10.1609/aiide.v18i1.21959. URL https://ojs.aaai.org/index.php/AIIDE/article/view/21959. Number: 1.

Volodymyr Mnih, Koray Kavukcuoglu, David Silver, Andrei A. Rusu, Joel Veness, Marc G. Bellemare, Alex Graves, Martin Riedmiller, Andreas K. Fidjeland, Georg Ostrovski, Stig Petersen, Charles Beattie, Amir Sadik, Ioannis Antonoglou, Helen King, Dharshan Kumaran, Daan Wierstra, Shane Legg, and Demis Hassabis. Human-level control through deep reinforcement learning. *Nature*, 518(7540):529–533, February 2015. ISSN 1476-4687. doi: 10.1038/nature14236. URL https://www.nature.com/articles/nature14236. Publisher: Nature Publishing Group.

Kevin P. Murphy. *Probabilistic Machine Learning: Advanced Topics*. MIT Press, 2023. URL http://probml.github.io/book2.

Antonin Raffin. Rl baselines3 zoo. https://github.com/DLR-RM/rl-baselines3-zoo, 2020.

Ashish Rao, Bidipta Sarkar, and Tejas Narayanan. Gaussian Process Policy Optimization, March 2020. URL http://arxiv.org/abs/2003.01074. arXiv:2003.01074 [cs, stat].

C. Rasmussen and M. Kuss. Gaussian Processes in Reinforcement Learning. December 2003. URL https://www.semanticscholar.org/paper/Gaussian-Processes-in-Reinforcement-Learning-Rasmussen-Kuss/3cc0095b47615c2f47beaca9bd8f675811fb118a.

Carl Edward Rasmussen and Christopher K. Williams. *Gaussian Processes for Machine Learning*. The MIT Press, Cambridge, 2019. ISBN 978-0-262-25683-4. OCLC: 1178958074.

Hugh Salimbeni and Marc Deisenroth. Doubly Stochastic Variational Inference for Deep Gaussian Processes, November 2017. URL http://arxiv.org/abs/1705.08933. arXiv:1705.08933 [stat].

John Schulman, Filip Wolski, Prafulla Dhariwal, Alec Radford, and Oleg Klimov. Proximal Policy Optimization Algorithms, August 2017. URL http://arxiv.org/abs/1707.06347. arXiv:1707.06347 [cs].

John Schulman, Philipp Moritz, Sergey Levine, Michael Jordan, and Pieter Abbeel. High-Dimensional Continuous Control Using Generalized Advantage Estimation, October 2018. URL http://arxiv.org/abs/1506.02438. arXiv:1506.02438 [cs].

Michalis Titsias. Variational Learning of Inducing Variables in Sparse Gaussian Processes. In *Proceedings of the Twelth International Conference on Artificial Intelligence and Statistics*, pages 567–574. PMLR, April 2009. URL https://proceedings.mlr.press/v5/titsias09a.html. ISSN: 1938-7228.

Mark Towers, Ariel Kwiatkowski, Jordan Terry, John U. Balis, Gianluca De Cola, Tristan Deleu, Manuel Goulão, Andreas Kallinteris, Markus Krimmel, Arjun KG, Rodrigo Perez-Vicente, Andrea Pierré, Sander Schulhoff, Jun Jet Tai, Hannah Tan, and Omar G. Younis. Gymnasium: A Standard Interface for Reinforcement Learning Environments, November 2024. URL http://arxiv.org/abs/2407.17032. arXiv:2407.17032 [cs].

Ziyu Wang, Tom Schaul, Matteo Hessel, Hado van Hasselt, Marc Lanctot, and Nando de Freitas. Dueling Network Architectures for Deep Reinforcement Learning, April 2016. URL http://arxiv.org/abs/1511.06581. arXiv:1511.06581 [cs].

A Experiment Setup

A.1 Environments

We trained the RL agents on two standard environments with continuous state and action spaces, Walker2D and Humanoid from the Gymnasium library Towers et al. [2024].

Walker2D. The Walker2D environment models a planar biped with 7 rigid links (torso, thighs, legs, feet) connected by 6 actuated joints. At each timestep, the agent observes a state $s_t \in \mathbb{R}^{17}$, consisting of joint angles and velocities (excluding global horizontal position), and outputs an action $a_t \in [-1, 1]^6$, representing torque commands for each joint. The reward at timestep t is given by

$$r_t = r_{\text{alive}} + r_{\text{velocity}} - \lambda \|a_t\|^2, \tag{13}$$

where $r_{\text{alive}} \in \{0, 1\}$ is a survival bonus, $r_{\text{velocity}} > 0$ rewards forward movement, and the final term penalizes taking actions that are too large with weight $\lambda = 10^{-3}$. Episodes terminate upon loss of balance, defined by the vertical position or orientation of the torso exceeding predefined thresholds.

Humanoid. The Humanoid environment models a 3D bipedal robot designed to simulate a human, with a torso, arms, and legs connected via 17 actuated hinge joints. At each timestep, the agent observes a state $s_t \in \mathbb{R}^{348}$ (by default, excluding global x- and y-coordinates), including positions, velocities, and inertia-related features of the robot's body parts, and outputs an action $a_t \in [-0.4, 0.4]^{17}$, representing torques applied at each joint. The reward at timestep t is

$$r_t = r_{\text{alive}} + r_{\text{forward}} - r_{\text{ctrl}} - r_{\text{contact}}, \tag{14}$$

where r_{alive} is a survival bonus, r_{forward} rewards forward motion, and the last two terms penalize large actions and excessive contact forces, respectively. Episodes terminate if the humanoid falls (torso height outside a healthy range) or after 1000 timesteps.

Environment preprocessing. The state space is standardized:

$$s_{\text{norm}} = \text{clip}\left(\frac{s - \mu_s}{\sqrt{\sigma_s^2 + \nu}}, -c, c \right),$$

where μ_s, σ_s are the running mean and variance, $\nu > 0$ is a small constant and $c = 10$.

A.2 Hyperparameter Tuning

For PPO, we used the optimal hyperparameters from the StableBaselines3 implementation as documented by Raffin [2020], including the default network: two hidden layers (64 units, tanh) for both policy and value functions.

For GPPO, hyperparameters were tuned for the environments via Bayesian optimization by maximizing the return averaged over $N_{\text{eval}} = 50$ evaluation episodes using the expected improvement acquisition function for 25 trails with 16 for random initialization. Early stopping is triggered if after 3000 episodes a reward of at least 200 averaged over the last 50 episodes was not reached.

The range of hyperparameters that were optimized for GPPO are listed in Table 2, with differences between the two environments highlighted. The architecture choices were encoded as integers and are illustrated in Figure 3, 4, 5. Note that passing the output from one layer to the next differs from an MLP, e.g., there are no 'weights' at the edges. Given an input from the previous layer $\mathbf{x}_{\ell-1}$, each GP in the next layer is given the input $\mathbf{f}_\ell(\mathbf{x}_{\ell-1}) = (f_\ell^1(\mathbf{x}_{\ell-1}), \ldots, f_\ell^w(\mathbf{x}_{\ell-1}))^\top$ and the resulting random vector represents the output at that layer. Because the random vector differs per $\mathbf{x}_{\ell-1}$ it is also loosely referred to as a random function.

A.3 Experiment Setup

We trained PPO and GPPO with an RTX 4090 for $N_1 = 10,000$ episodes on the Walker2D environment and $N_2 = 15,000$ episodes in Humanoid with the respective optimized hyperparameters. This was repeated for 3 runs for Walker2D in order to obtain statistically robust results. All experiments were conducted using a 8 parallel environment instances.

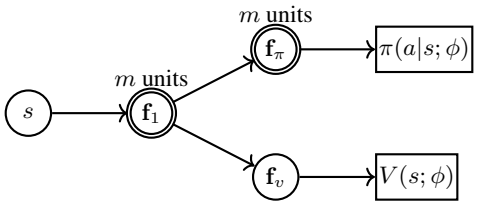

Figure 3: Architecture 0: Shared layer with m GP units (corresponding to the number of actions) feeding into the policy head (m GPs) and value head (single GP). Double circles indicate multiple GP units in a layer.

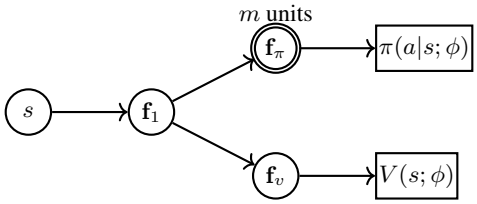

Figure 4: Architecture 1: Single shared GP feeding into the policy head with m GPs (for the m actions) and value head (single GP).

We visualized return variability across runs using interquartile mean (IQM) reward curves with 95% bootstrap confidence intervals (CIs). Let $g_{i,t}$ be the return of run i at episode t, and $\{g_{1,t}, \ldots, g_{M,t}\}$ the sorted set. Define $k = \lfloor 0.25M \rfloor$; the IQM at episode t is:

$$\text{IQM}_t = \frac{1}{M - 2k} \sum_{j=k+1}^{M-k} g_{(j),t}. \tag{15}$$

We resample M runs with replacement $B = 100$ times to compute a bootstrap distribution $\{\text{IQM}_b^*\}_{b=1}^B$, from which we extract the $(\alpha/2, 1-\alpha/2)$ percentiles to form the $1-\alpha$ CI:

$$\text{CI} = \left[\text{IQM}^*_{(\alpha/2)}, \text{IQM}^*_{(1-\alpha/2)}\right]. \tag{16}$$

Compared to the mean $\pm$ standard deviation, which is sensitive to outliers and assumes Gaussianity, IQM with bootstrap CIs offers a more robust summary of performance, especially with few runs (e.g., 3–10), by averaging the central 50% and estimating uncertainty non-parametrically Agarwal et al. [2021].

After training we conduct a brief 100 episode evaluation run.

B Complexity

We empirically estimate the time complexity by comparing execution time during training. We run a smaller training loop of 100 episodes and compute the mean and standard deviation of the action sampling latency and training update latency. The hyperparameters are the same as used during full training except that the number of environments was set to 1. This implies the max buffer size is equal to `n_steps`. Note that in general, there is a speedup when training on multiple environments in parallel. The results are in Table 4.

C Additional caveats/implementation details

When modeling the policy as the predictive distribution of a DGPs there are some consequences. We considering the case where we are using DSPPs with a Gaussian likelihood.

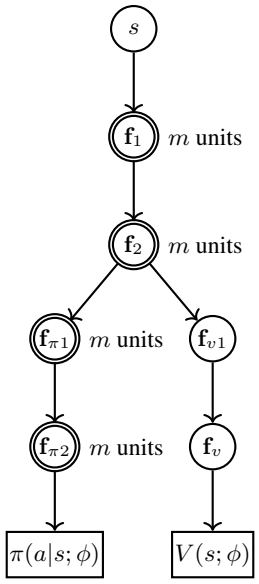

Figure 5: Architecture 2: Two shared layers with m GP units (for m actions) feeding the policy head (two m-GP layers) and value head (single GP). Double circles indicate multiple GP units.

Table 2: Bayesian Hyperparameter Optimization Setup for GPPO.

Hyperparameter	**Value or Range**
Agent type	Fixed: GPPO
Architecture Choice	0–2
Batch size	Fixed: 512
`n_steps`	64-512 (int)
`n_envs`	Fixed: 8
Training episodes (N)	Fixed: 3000 (Inv. Pendulum) Fixed: 10,000 (Walker2D)
Evaluation episodes (N_{eval})	Fixed: 50
Learning rate	10^{-5}–10^{-2} (log scale)
Number of epochs	1–10 (int)
Discount factor (γ)	Fixed: 0.999
GAE lambda	Fixed: 0.9 (Inv. Pendulum)
Clip range (ϵ)	0.1–0.4 (float)
Entropy coefficient (c_2)	10^{-7}–10^{-1} (log scale)
Value function coefficient (c_2)	0.2–1.0 (float)
Max gradient norm ($\|g\|_{\max}$)	0.2–1.0 (float)
Number of inducing points (M)	128–256 (int)
Number of quadrature sites (Q)	Fixed: 8
KL. div. coefficient (β)	Fixed: 1
Optimizer	Fixed: Adam

Entropy calculation: If a neural network outputs a multivariate Gaussian $\pi(a|s;\theta) = \mathcal{N}(a|\mu_\theta(s), \Sigma_\theta(s))$ then the entropy $\mathcal{H}[\pi(a|s;\theta)]$ can be computed in closed form:

$$\begin{aligned}&\mathcal{H}[\mathcal{N}(a|\mu_\theta(s), \Sigma_\theta(s))] \\ &\quad = \tfrac{1}{2}\log\left((2\pi e)^D \det \Sigma_\theta(s)\right) \\ &\quad = \tfrac{D}{2}(1+\log(2\pi)) + \tfrac{1}{2}\log\det\Sigma_\theta(s).\end{aligned} \tag{17}$$

Table 3: Hyperparameters for PPO and GPPO on Walker2D and Humanoid. GPPO hyperparameters were obtained through Bayesian optimization, while PPO hyperparameters were based on the optimal configuration for the StableBaselines3 implementation. Explanation of additional hyperparameters for GPPO: *Inducing points* = number of points used in sparse GP approximation per GP unit; *Quadrature sites* = number of learnable sigma points in DSPPs; β = KL-penalty weight of KL divergence between prior distribution over inducing variables and the approximate posterior.

Hyperparameter	**Walker2D**		**Humanoid**	
	PPO	GPPO	PPO	GPPO
Architecture choice	-	3	-	3
Steps per update (`n_steps`)	256	286	256	249
Batch size	512	512	256	256
Learning rate	5.05×10^{-5}	2.54×10^{-3}	3.57×10^{-5}	1.95×10^{-3}
Number of epochs	20	9	5	10
Discount factor (γ)	0.99	0.999	0.95	0.95
GAE lambda (λ)	0.95	0.9	0.9	0.9
Clip range (ϵ)	0.1	0.156	0.3	0.348
Value function coefficient (c_1)	0.872	0.574	0.432	0.919
Entropy coefficient (c_2)	5.85×10^{-4}	2.01×10^{-6}	2.38×10^{-3}	8.7×10^{-5}
Max grad norm	1.0	0.667	2.0	0.870
# Inducing points (M)	–	128	–	128
Quadrature sites (Q)	–	8	–	8
KL div. coefficient (β)	–	1	–	1

Environment	**Algorithm / Stage**	**Mean $\pm$ Std. Dev.**
Walker2d-v5	GPPO - Inference (per step)	13.752 ms $\pm$ 23.867 ms
	GPPO - Training (per update)	0.403 s $\pm$ 0.013 s
	PPO - Inference (per step)	1.810 ms $\pm$ 7.831 ms
	PPO - Training (per update)	0.089 s $\pm$ 0.072 s
Humanoid-v5	GPPO - Inference (per step)	14.324 ms $\pm$ 29.732 ms
	GPPO - Training (per update)	0.445 s $\pm$ 0.033 s
	PPO - Inference (per step)	1.938 ms $\pm$ 8.497 ms
	PPO - Training (per update)	0.051 s $\pm$ 0.092 s

Table 4: Timing metrics summary for Walker2d-v5 and Humanoid-v5 comparing GPPO and standard PPO. Values are reported as mean $\pm$ standard deviation for inference and training times.

Where D is the dimensionality of the action space. For a diagonal covariance matrix $\Sigma_\theta(s) = \text{diag}(\sigma^2_\theta(s))$, this simplifies to:

$$\mathcal{H}[\mathcal{N}(a|\mu_\theta(s), \Sigma_\theta(s))] = \frac{D}{2}(1 + \log(2\pi)) + \frac{1}{2}\sum_{d=1}^{D} \log \sigma^2_{\theta,d}(s). \tag{18}$$

In contrast, with DGPs we cannot compute the entropy in closed form. An unbiased Monte carlo estimate can be obtained usng:

$$\mathcal{H}[\pi(a|s;\phi)] \approx -\frac{1}{B}\sum_{i=1}^{B} \log \pi(a_i|s_i;\phi). \tag{19}$$

Where B is the number of trajectories.

Sampling actions: In contrast to policies represented by a single Gaussian distribution, the predictive distribution of a DSPP with a Gaussian likelihood is a mixture of Gaussians with Q components. This differs from standard neural network policies, which output a single Gaussian:

$$\pi(a|s;\theta) = \mathcal{N}\left(a|\mu_\theta(s), \Sigma_\theta(s)\right). \tag{20}$$

Sampling from this Gaussian is straightforward using the reparameterization trick:

$$a = \mu_\theta(s) + \Sigma_\theta^{1/2}(s)\,\epsilon, \quad \epsilon \sim \mathcal{N}(0, I). \tag{21}$$

For the DSPP policy, however, sampling involves two steps:

1. **Component selection:** Sample an index $q \sim \text{Categorical}(\omega_1(s), \ldots, \omega_Q(s))$.
2. **Gaussian sampling:** Given component q, sample $a \sim \mathcal{N}(\mu_q(s), \Sigma_q(s))$ (using the reparameterization trick).

The resulting distribution $\pi(a|s;\phi)$ is non-Gaussian and can be *multi-modal* or *heavy-tailed*, allowing the policy to model richer uncertainties and more complex behaviors than a unimodal Gaussian.

Sampling the value function: In standard PPO, the value function is a deterministic regressor, typically trained with squared error loss. Its output is a point estimate, which is used in the GAE framework to compute advantage values $\hat{A}_t$. However, in GPPO, we model the value function as a posterior distribution over values conditioned on state inputs.

This formulation enables us to capture uncertainty in the value predictions, both epistemic (model uncertainty due to limited data) and aleatoric (inherent noise). Instead of computing advantages using only the mean prediction $\bar{V}_\phi(s)$, we can propagate this uncertainty into the policy update step by sampling from the value function posterior $\tilde{V}(s) \sim p_{\text{dspp}}(V^{\text{target}}|s;\phi)$. These samples are then used to compute a stochastic estimate of the GAE. Since $\tilde{V}_\phi(s)$ is now stochastic, each sampled trajectory yields a different $\hat{A}_t$, effectively turning the advantage into a random variable. This has several important consequences:

- **Implicit exploration signal:** The variance in $\hat{A}_t$ introduces a natural exploration mechanism. If the value estimate is uncertain (e.g., in regions of the state space not well observed), the sampled $\hat{A}_t$ values can vary widely. Guiding the policy to explore uncertain states.
- **Adaptive advantage scaling:** Uncertainty-aware sampling causes the magnitude of $\hat{A}_t$ to reflect not just expected return, but confidence. High-confidence states result in stable $\hat{A}_t$, while low-confidence regions exhibit noisy but potentially high-magnitude $\hat{A}_t$.